CHINESE OPTICS LETTERS

Vol. 21, No. 10 | October 2023

Low-cost spectrometer design for ultra-high resolution spectral domain optical coherence tomography

Chaoliang Chen (陈朝良)[1*], Yurui Pu (蒲郁蕊)[1], and Weisong Shi (史伟松)[2]

[1] Advanced Photonics Center, School of Electronic Science & Engineering, Southeast University, Nanjing 210096, China

[2] Department of Optical Engineering, Nanjing University of Science and Technology, Nanjing 210094, China

*Corresponding author: chaoliangchen@seu.edu.cn

Received January 4, 2023 | Accepted May 5, 2023 | Posted Online August 30, 2023

In this Letter, we present a low-cost, high-resolution spectrometer design for ultra-high resolution optical coherence tomography (UHR-OCT), in which multiple standard achromatic lenses are combined to replace the expensive F-theta lens to achieve a comparable performance. For UHR-OCT, the spectrometer plays an important role in high-quality 3D image reconstruction. Typically, an F-theta lens is used in spectrometers as the Fourier lens to focus the dispersed light on the sensor array, and this F-theta lens is one of the most expensive components in spectrometers. The advantage of F-theta lens over the most widely used achromatic lens is that the aberrations (mainly spherical aberration, SA) are corrected, so the foci of the dispersed optical beams (at different wavelengths) with different incident angles could be placed on the sensor array simultaneously. For the achromatic lens, the foci of the center part of the spectrum are farther than those on the side in the longitudinal direction, causing degradations of the spectral resolution. Furthermore, in comparison with the achromatic lens with the same focal length, those with smaller diameters have stronger SA, but small lenses are what we need for making spectrometers compact and stable. In this work, we propose a simple method of using multiple long-focal-length achromatic lenses together to replace the F-theta lens, which is $>$8-fold cheaper based on the price of optical components from Thorlabs, US. Both simulations and *in vivo* experiments were implemented to demonstrate the performance of the proposed method.

Keywords: low-cost spectrometer; optical coherence tomography; spherical aberration suppression; ultrahigh-resolution non-invasive imaging.

DOI: 10.3788/COL202321.101101

1. Introduction

Optical coherence tomography (OCT) is an imaging modality proposed in 1990s[1], and it is now broadly applied in various fields, such as ophthalmology[2,3], dermatology[4,5], and gastroenterology[6,7]. One advantage of this technique is its high-resolution imaging, which is achieved with the interference of the broadband spectrum. In Fourier domain OCT systems, the typically used light sources for spectral domain OCT (SDOCT)[8] and swept source OCT (SSOCT)[9] are, respectively, a superluminescent diode (SLD) and a swept source, where an optoelectronic diode is used for the stimulated emission in both situations. Due to the limited bandwidth of the optoelectronic diodes, a typically achieved axial resolution is ~10 μm. To further improve the resolution, a supercontinuum (SC) light source was first used to achieve ultra-high resolution imaging at the micron order, termed as ultra-high resolution optical coherence tomography (UHR-OCT)[10]. SC-based UHR-OCT has a relatively lower sensitivity compared to optoelectronic diode-based systems due to its less stable power spectral density[11]. Another method commonly used to achieve a large spectral bandwidth is to combine multiple SLDs[12], which costs less when compared to SC-based UHR-OCT and could maintain the imaging sensitivity.

For SDOCT, one of the key components for high-quality imaging is the high-resolution spectrometer, in which a collimated beam could be dispersed and focused on a line-array sensor for interference fringes capture. The performance of the spectrometer is determined by the spot size of the different wavelength components on the line-array sensor. The less overlap there is between the wavelength ranges of the two adjacent sensor pixels, the higher fringes contrast. Therefore, many spectrometer designs have recently been proposed to improve the performance. For example, Lee *et al.* designed and fabricated an F-theta lens and used it in the spectrometer as the Fourier lens (the lens just before the line-array sensor) to correct the field

curvature aberration, achieving improved sensitivity fall-off as imaging depth increases[13]. Wu *et al.* performed a prism and a multi-element scan lens to achieve a high-resolution and wavenumber-linear spectrometer, which could skip fringe resampling during data processing process[14]. Wang *et al.* used a concave mirror instead of a lens in the spectrometer to improve the transmission efficiency[15], achieving improved signal-to-noise ratio and sensitivity. However, in the above mentioned reports, a complicated optical design, an optical manufacturing, or a system structure is needed, making the system more expensive or optical components alignment more challenging.

In the standard structure of spectrometers, the challenging part is to make the dispersed beam foci after the Fourier lens reach the line-array sensor simultaneously, and one of the commonly used methods is to apply an F-theta lens (which has a flat imaging field) as the Fourier lens, such as Lee *et al.*'s work[13].

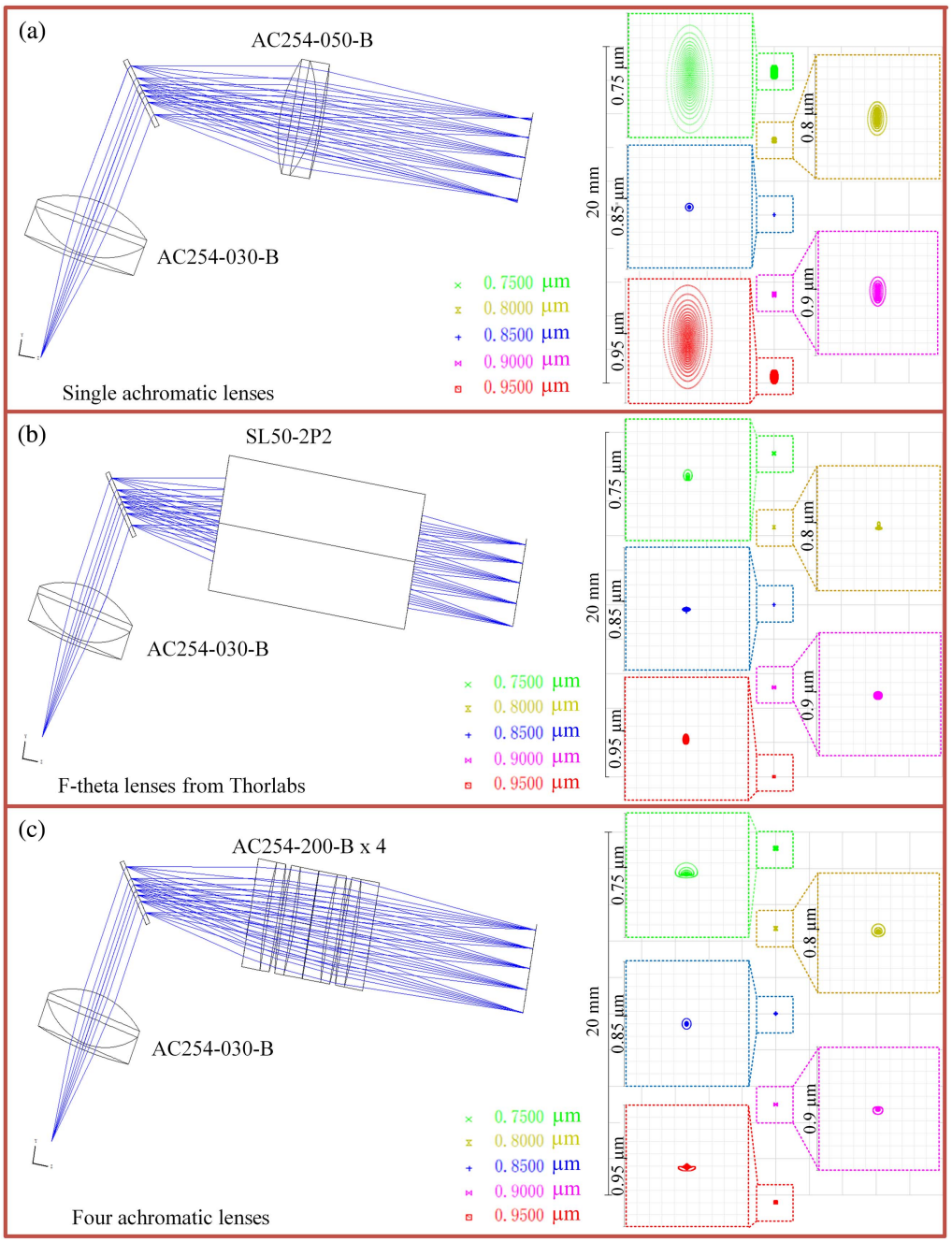

Fig. 1. The simulations with Zemax ray tracing software. (a) The spectrometer with one achromatic lens (EFL = 50 mm) used to replace the F-theta lens. (b) The spectrometer with a typical F-theta lens (EFL = 50 mm, SL50-2P2, Thorlabs, NJ, USA). (c) The spectrometer with the combined 4 achromatic lenses (EFL = 50 mm) used to replace the F-theta lens. The spot diagrams at the five representative wavelengths (0.75 μm, 0.8 μm, 0.85 μm, 0.9 μm, and 0.95 μm) on the line-array sensor plane are shown for comparison in (a)–(c). The RMS radii of the spot diagrams are shown in Table 1.

However, an F-theta lens typically costs ~10-fold more than an achromatic lens of the same size based on the price from Thorlabs, US. For the achromatic lens, the off-center light arrays are always refracted more than those close to the center (called spherical aberration, SA), causing the foci of the dispersed beams not to be in the same plane, which limits the performance of spectrometers. Because SA relieves as the curvature of the refractive surface drops, we could combine multiple lenses with longer focal lengths to achieve an SA-suppressed short focal length lens.

In this Letter, we present a low-cost, high-resolution spectrometer design for UHR-OCT, in which multiple standard achromatic lenses with longer focal lengths are combined to suppress SA and to replace the F-theta lens without image-quality degradation, achieving a $>$ 8-fold less cost compared to a typical F-theta lens. Both simulations and experiments were performed to verify and validate the proposed method.

2. Method

Figure 1 shows the comparison of simulations with Zemax ray tracing software for the spectrometers with three kinds of Fourier lenses: the single achromatic lens, the F-theta lens, and the combined four achromatic lenses. The effective focal length (EFL) for all three Fourier lenses is 50 mm. In the design, the collimating lens is an achromatic lens with a focal length of 30 mm. The grating has a resolution of 1500 lp/mm with a thickness of 1 mm. All the parameters of the optical lenses are obtained from Thorlabs, US. From the left panel of Fig. 1(a), we can see that the distributions of the foci of the five representative wavelengths (750 nm, 800 nm, 850 nm, 900 nm, and 950 nm) are not flat and could not reach the line-array sensor simultaneously, causing spectral resolution degradation on both sides of the line-array sensor, which agrees with the above-mentioned fundamentals. For the other two settings, the foci of the mentioned five wavelengths reach the line-array sensor almost at the same time, and the performances are comparable to each other. The right panels of Figs. 1(a)–1(c) are the magnified spot diagrams of the five wavelengths on the sensor array plane, and the root-mean-square (RMS) radii of the five diagrams are shown in Table 1. Comparing these values, we can see that the performances of the F-theta lens and the combined four achromatic lenses are close to each other and are much better than the single achromatic lens.

Table 1. The Comparison of the Root-Mean-Square (RMS) Radius at the Five Specific Wavelengths.

	RMS Radius (μm)		
Wavelength (nm)	Single Achromatic Lens	F-theta Lens	Combination of Four Achromatic Lenses
750	156.5	15.1	26.7
800	43.4	13.7	16.6
850	10.0	16.4	12.8
900	36.0	20.7	13.4
950	149.6	21.4	19.5

As illustrated in Fig. 2, we built an SDOCT system in our lab to verify and validate the results of the simulations, in which the light source is an SLD (cBLMD-T-850-HP-I, SUPERLUM, Ireland) centered at 850 nm with a 3 dB bandwidth of 165 nm, achieving an axial resolution of ~1.93 μm in air and ~1.5 μm in tissue with a typical refractive index of 1.3. The structure of the system is a Michelson interferometer, and a 50:50 fiber coupler splits the optical beam into a reference beam and a sample beam. The photons reflected from the reference arm and backscattered from the sample interfere at the coupler and are forwarded to a customized high-resolution spectrometer for signal detection, where 4 standard achromatic lenses are combined to be used as the Fourier lens. The collimating lenses L1 and L2 in the reference and sample arms, respectively, have a focal length of 19 mm. The objective lens L3 also has a focal lens of 19 mm, achieving a lateral resolution of ~3.9 μm[16]. The collimating lens L4 has a focal length of 30 mm, and the combined

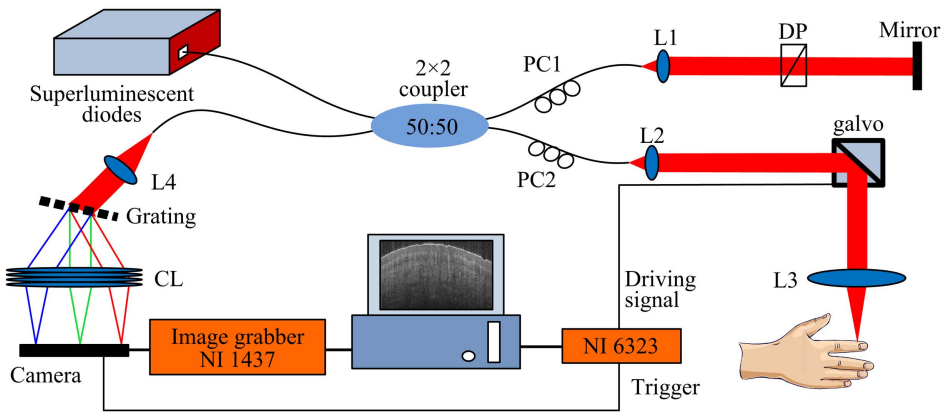

Fig. 2. The schematic of the home-built SDOCT system. PC1, PC2: polarization controllers; DP: dispersion compensation pair; L1–L4: achromatic lenses; CL: combination of four achromatic lenses. The CL is obtained by putting the four lenses together in one single-lens mounting tube.

lens (CL) is composed of 4 achromatic lenses (with a focal length of 200 mm), and the EFL of the CL is 50 mm. The grating (FSTG-NIR1500-908, Ibsen, UK) has a resolution of 1500 lp/mm. The line-array sensor is a line-scan camera (2048 pixels, OCTOPLUS, E2V, UK) with an A-line rate of 130 kHz at a pixel depth of 12 bits. In our system setup, the optical power outputted from the sample arm and exposed on the sample is ~2.5 mW. The measured axial resolution calculated by fitting the PSF with a Gaussian function is ~2.6 μm in air, which agrees with the theoretical value, and the achieved full imaging depth range in air is ~1.9 mm.

In this work, the spectrum measured by the home-built spectrometer is calibrated with a method similar to Wang *et al.*'s work[17]. A piece of cover slip with a thickness of $d = 180$ μm is placed in the sample arm to acquire the interference fringes, and then the Hilbert transform is performed on the fringes to calculate the complex analytic signals. After that, the phase signal φ of the interference fringes can be obtained. A laser beam at 0.85 μm from a laser diode is forwarded to the spectrometer to get the pixel index j at 0.85 μm. The phase offset for the obtained phase signal φ can then be obtained by

$$\mathrm{d}\varphi = 2\pi \cdot \left(\left\lfloor \frac{2d \cdot n}{0.85} \right\rfloor - \left\lfloor \frac{\varphi(j)}{2\pi} \right\rfloor \right), \tag{1}$$

where n is the refractive index of the coverslip, and the operator $\lfloor\rfloor$ represents the floor function. The phase signal of the interference fringes of the cover slip can then be obtained by adding the phase signal, and the phase offset $\varphi' = \varphi + \mathrm{d}\varphi$. Finally, the wavelength at each pixel of the camera can be obtained by

$$\lambda = 4\pi \cdot d \cdot n/\varphi', \tag{2}$$

where λ is the wavelength. Furthermore, numerical dispersion compensation[18] is performed in this work to compensate the dispersion mismatch between the sample and reference arms.

3. Results and Discussions

Figure 3 shows the results obtained with our home-built SDOCT system. Figure 3(a) shows the normalized power spectral density obtained by our customized high-resolution spectrometer. Figure 3(b) shows the reference plot of the normalized power spectral density from the user manual of the light source. In comparing Figs. 3(a) and 3(b), it can be seen that the spectrum measured by the customized spectrometer generally matches with the reference data, but the intensity of the spectrum on both edges is slightly weaker compared to the reference data. This is caused by the accumulated spectral filtering of the optical components, such as fiber coupler and lenses. Figure 3(c) shows the point spread functions (PSFs) at different depths, and an optical neutral density filter with an OD of 2 was inserted into the sample arm. The different optical path length difference (OPD) was achieved by varying the OPD of the reference arm. The system achieves a sensitivity of ~100 dB around zero OPD and a

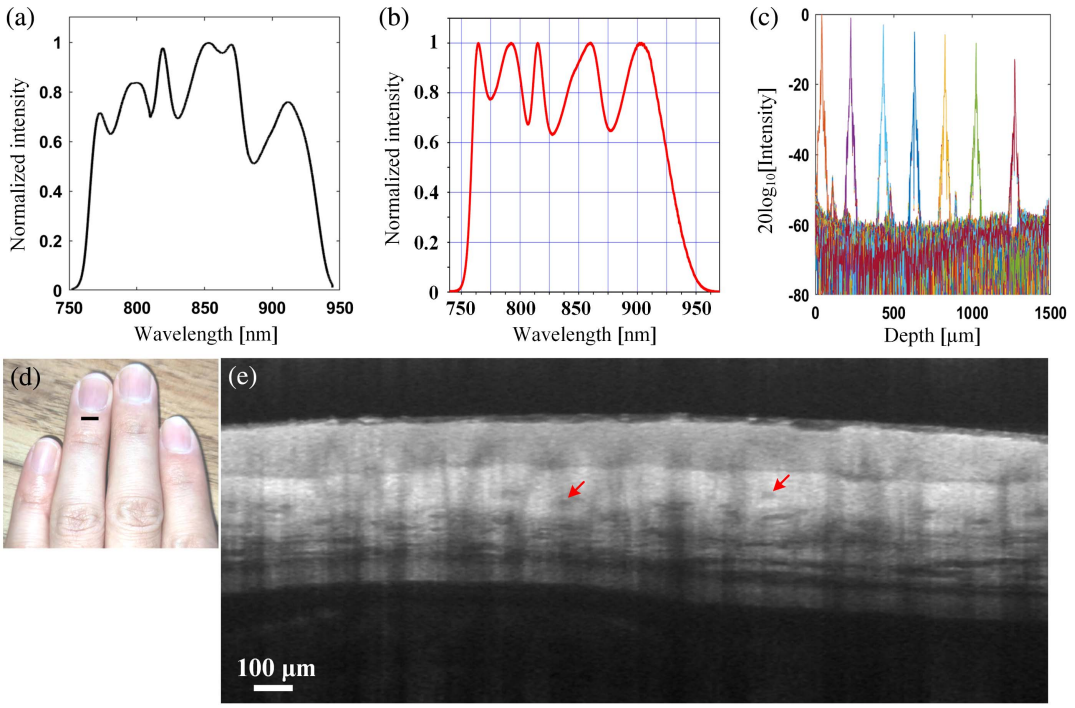

Fig. 3. The results of the home-built SDOCT system. (a) The normalized power spectral density obtained by the customized spectrometer. (b) The reference data of the normalized power spectral density from the user manual of light source. (c) The point spread functions (PSFs) at different depths with an optical neutral density filter (OD = 2) inserted in the sample arm. (d) A healthy volunteer's finger, and the marked position was scanned. (e) A 10 B-scans averaged structural image obtained by the proposed low-cost high-resolution spectrometer. The marked positions are blood vessels.

sensitivity drop-off of ~8 dB/mm, which meets the requirement of clinical imaging systems. Figure 3(e) shows a high-resolution structural image (with 10 B-scans averaged) of a healthy volunteer's fourth finger at the marked position in Fig. 3(d). As a benefit of high-resolution, the blood vessels are marked by the red arrows and can be clearly seen.

For spherical lens, SA is unavoidable because off-center light rays are refracted more than those close to the center. To shorten the focal length of spherical lens, the curvatures of the surfaces need to be increased, and the SA is more severe in this case. In this work, four lenses with a focal length of 200 mm are combined to achieve an equivalent lens with an EFL of 50 mm without improving the curvatures of any refractive spherical surfaces, and the obtained performance is comparable to the F-theta lens.

In Fig. 3(c), the full width at half-maximum (FWHM) of the PSFs at different depths slightly varies. This may be caused by the laser diode used in the spectrometer calibration process because the laser diode used in this work is a regular laser diode whose center wavelength drifts as the temperature changes. The calibration accuracy could be improved by using a standard light source instead.

4. Conclusion

In summary, this work presents a low-cost design for the high-resolution spectrometer for ultra-high resolution optical coherence tomography (UHR-OCT), in which four standard achromatic lenses are combined to replace the expensive F-theta lens. Both simulations and *in vivo* experiments were implemented to test the proposed method, and the obtained results demonstrate that this method could reach a comparable performance to a typical F-theta lens. Because OCT demands relatively expensive clinical devices, we believe this work could help reduce the cost for clinical systems, and it could be helpful to the resources-limited researchers as well.

Acknowledgement

This work was supported by the Natural Science Foundation of Jiangsu Province (No. BK20210227).

References

1. D. Huang, E. A. Swanson, C. P. Lin, J. S. Schuman, W. G. Stinson, W. Chang, M. R. Hee, T. Flotte, K. Gregory, C. A. Puliafito, and J. G. Fujimoto, "Optical coherence tomography," Science **254**, 1178 (1991).
2. W. Drexler and J. G. Fujimoto, "State-of-the-art retinal optical coherence tomography," Prog. Retin. Eye Res. **27**, 45 (2008).
3. D. M. Sampson, A. M. Dubis, F. K. Chen, R. J. Zawadzki, and D. D. Sampson, "Towards standardizing retinal optical coherence tomography angiography: a review," Light Sci. Appl. **11**, 63 (2022).
4. C. Chen, K. H. Y. Cheng, R. Jakubovic, J. Jivraj, J. Ramjist, R. Deorajh, W. Gao, E. Barnes, L. Chin, and V. X. D. Yang, "High speed, wide velocity dynamic range Doppler optical coherence tomography (Part V): optimal utilization of multi-beam scanning for Doppler and speckle variance microvascular imaging," Opt. Express **25**, 7761 (2017).
5. J. Olsen, J. Holmes, and G. B. E. Jemec, "Advances in optical coherence tomography in dermatology—a review," J. Biomed. Opt. **23**, 040901 (2018).
6. G. J. Tearney, M. E. Brezinski, J. F. Southern, B. E. Bouma, S. A. Boppart, and J. G. Fujimoto, "Optical biopsy in human gastrointestinal tissue using optical coherence tomography," Am. J. Gastroenteral. **92**, 1800 (1997).
7. J. Zhang, T. Nguyen, B. Potsaid, V. Jayaraman, C. Burgner, S. Chen, J. Li, K. Liang, A. Cable, G. Traverso, H. Mashimo, and J. G. Fujimoto, "Multi-MHz MEMS-VCSEL swept-source optical coherence tomography for endoscopic structural and angiographic imaging with miniaturized brushless motor probes," Biomed. Opt. Express **12**, 2384 (2021).
8. R. Leitgeb, M. Wojtkowski, A. Kowalczyk, C. K. Hitzenberger, M. Sticker, and A. F. Fercher, "Spectral measurement of absorption by spectroscopic frequency-domain optical coherence tomography," Opt. Lett. **25**, 820 (2000).
9. S. H. Yun, C. Boudoux, G. J. Tearney, and B. E. Bouma, "High-speed wavelength-swept semiconductor laser with a polygon-scanner-based wavelength filter," Opt. Lett. **28**, 1981 (2003).
10. L. Liu, J. A. Gardecki, S. K. Nadkarni, J. D. Toussaint, Y. Yagi, B. E. Bouma, and G. J. Tearney, "Imaging the subcellular structure of human coronary atherosclerosis using micro–optical coherence tomography," Nat. Med. **17**, 1010 (2011).
11. C. Chen, W. Shi, R. Reyes, and V. X. D. Yang, "Buffer-averaging super-continuum source based spectral domain optical coherence tomography for high speed imaging," Biomed. Opt. Express **9**, 6529 (2018).
12. R. Haindl, M. Duelk, S. Gloor, J. Dahdah, J. Ojeda, C. Sturtzel, S. Deng, A. J. Deloria, Q. Li, M. Liu, M. Distel, W. Drexler, and R. Leitgeb, "Ultra-high-resolution SD-OCM imaging with a compact polarization-aligned 840 nm broadband combined-SLED source," Biomed. Opt. Express **11**, 3395 (2020).
13. S. S. Lee, W. Song, and E. S. Choi, "Spectral domain optical coherence tomography imaging performance improvement based on field curvature aberration-corrected spectrometer," Appl. Sci. **10**, 3657 (2020).
14. W. Yu, J. Mavadia-Shukla, J. Xi, W. Liang, X. Yu, S. Yu, and X. Li, "Optimal operational conditions for supercontinuum-based ultrahigh-resolution endoscopic OCT imaging," Opt. Lett. **41**, 250 (2016).
15. L. Wang, X. Yu, X. Ge, X. Wu, X. Wang, E. Bo, N. Wang, X. Liu, G. Ni, and L. Liu, "Design and optimization of a spectrometer for high-resolution SD-OCT," Laser Phys. Lett. **16**, 045603 (2019).
16. J. A. Izatt and M. A. Choma, "Theory of Optical Coherence Tomography," in *Optical Coherence Tomography: Technology and Applications*, W. Drexler and J. Fujimoto, eds., Vol. **2** (Springer, 2015), p. 65.
17. K. Wang and Z. Ding, "Spectral calibration in spectral domain optical coherence tomography," Chin. Opt. Lett. **6**, 902 (2008).
18. A. F. Fercher, C. K. Hitzenberger, M. Sticker, R. Zawadzki, B. Karamata, and T. Lasser, "Numerical dispersion compensation for partial coherence interferometry and optical coherence tomography," Opt. Express **9**, 610 (2001).